Enhanced Enzyme Immobilization Using a Novel Agarose-binding Tag Leads to Improved Flow Reactor Performance

Martin Peng,[a] Matthias Franzreb,[b] Annika J. Weber,[a] Phillip Lemke,[a] Christof M. Niemeyer,[a] and Kersten S. Rabe*[a]

Continuous enzymatic synthesis has gained increasing prominence, extending its applicability to the chemical industry. A practical approach for integrating enzymes into continuously operated reactors is their entrapment within polymer-based hydrogels. In this study, we present a novel approach to enhance enzyme retention within agarose hydrogels, employing a carbohydrate-binding module sourced from the *Microbulbifer thermotolerans* thermostable β-agarase I (MtCBM) as a versatile agarose-binding tag. Among the four tested carbohydrate-binding modules, MtCBM exhibited superior binding affinity to solid agarose and fusion proteins incorporating MtCBM demonstrated significantly enhanced retention within agarose hydrogels. Employing a newly developed fluidic flat-bed agarose reactor, we demonstrate that, due to increased retention in agarose hydrogels, a phenacrylate decarboxylase tagged with MtCBM yielded nearly six times more product compared to a similarly sized fusion enzyme lacking the MtCBM-tag. The higher leaching rate of the unlabeled enzyme could not be compensated even by tripling the hydrogel layer thickness, clearly documenting the effectiveness of MtCBM labeling for retention in the gel matrix. In addition, we performed theoretical modelling of the reactor, which led to a deeper understanding of the retention kinetics. The results suggest that this innovative approach is promising for improving stability and reusability of enzymes in agarose-based carriers.

Introduction

Enzymes play a crucial role in many biological processes and their ability to perform reactions with high efficiency and specificity made them valuable catalytic tools for many chemical transformations in industrial applications.[1,2] To overcome challenges such as low process stability of enzymes and limited reusability, as well as to enable continuous substrate conversion in flow reactors, enzymes can be immobilized.[2,3] In this context, encapsulation or entrapment of enzymes in polymer-based hydrogels is a simple and well-established way to achieve enzyme immobilization by pure physical retention of the catalyst.[4–8] However, enzyme leaching as well as mass transfer limitation due to elongated diffusion length must be considered.[9,10] The mass transfer can be improved by using hydrogels with minimal diffusion paths.[11] Here, 3D printing of hydrogels offers a way of simple and efficient rapid prototyping that allows the optimization of diffusion paths.[9,12,13] In partic-

ular, agarose-based hydrogels can by employed for 3D printing,[6–8] and they can also be used for a variety of other methods to achieve defined 3D structures, such as continuous microdroplet generation,[14] layer-by-layer fabrication[15] and advanced casting.[16,17] Hydrogel-forming polymers such as agarose or alginate offer advantages such as their biodegradability, renewability and non-toxicity, and their properties such as gelling behavior can be further tailored by using chemically modified polymers as well as polymer blends.[16,18]

In a previous work, we established the extrusion-based 3D printing of thermostable enzymes in an agarose matrix and realized multi-step, sequential biotransformations and chemo-enzymatic conversions in flow reactors.[6,7] However, since we found considerable enzyme leaching, an increased retention of the enzyme would be desirable to improve reactor efficiency. One strategy would be to increase the thickness of the printed agarose material, which however requires modification of the reactor design and also impacts the diffusion paths. Alternatively the retention of enzymes in the matrix can be increased using chemical crosslinking, however chemical modifications to covalently attach the enzymes to the material need additional post-processing steps, which can negatively impact the catalytic activity.[5,10] Using genetically encoded affinity-based tagging systems would be an elegant solution, which is fully compatible with existing reactor designs.[19] While well-established system that bind carbohydrates, like the chitin-binding domain from *Bacillus circulans*[20] and the maltose-binding protein from *Escherichia coli*,[21] would need to be reengineered to bind agarose, the available galactose-binding lectins from the slime mold *Dictyostelium discoideum*,[22] the earthworm *Lumbricus terrestris*[23] or the mushroom *Laetiporus sulphureus*[24] seem to be not useful as they show a dissociation constant with agarose

[a] M. Peng, A. J. Weber, P. Lemke, C. M. Niemeyer, K. S. Rabe
Institute for Biological Interfaces (IBG 1), Karlsruhe Institute of Technology (KIT), Hermann-von-Helmholtz-Platz 1, D-76344 Eggenstein-Leopoldshafen, Germany
E-mail: kersten.rabe@kit.edu

[b] M. Franzreb
Institute of Functional Interfaces (IFG), Karlsruhe Institute of Technology (KIT), Hermann-von-Helmholtz-Platz 1, D-76344 Eggenstein-Leopoldshafen, Germany

ChemCatChem

Research Article
doi.org/10.1002/cctc.202400092

Chemistry
Europe

European Chemical
Societies Publishing

of only about 1.7×10^{-4} M.[25] In contrast, due to their independent fold and modularity, carbohydrate-binding modules (CBMs) are an ideal class of proteins for the development of an agarose-binding tag, which show high specificity toward agarose and dissociation constants down to 6.6×10^{-6} M.[26,27] To evaluate the potential of CBMs as genetically encoded binding tags, we compared four different CBMs and then analyzed the binding properties of the best performing CBM in detail. Subsequently, we examined the retention characteristics of genetic fusions of a phenolic acid decarboxylase (PAD, EC 4.1.1.102) tagged with the identified optimal CBM. The analysis was carried out in flat-bed reactors equipped with agarose hydrogels of defined heights, operating under various flow rates. The acquired data was then utilized to simulate and evaluate the performance of the reactor.

Results and Discussion

In order to identify a suitable binding protein to be utilized as fusion partner for the attachment of enzymes to improve their retention in agarose hydrogels, four different CBM candidates with difference in their potential agarose binding properties were selected. CBM13 fold from *Catenovulum agarivorans* agarase YM01-3 (CaCBM)[28] offers up to three potential type C binding sites in a β-trefoil fold.[29] The CBM6 fold *Microbulbifer thermotolerans* agarase I (MtCBM)[30] and *Flammeovirga pacifica* AgaP4383 (FpCBM)[31] contains a primary binding site I with

either type B or type C binding properties,[32] and a potential second binding site II with cleft-like type B topology.[33–35] The fourth candidate was the CBM-like domain from *Saccharophagus degradans* agarase Aga50D (SdCBM),[36] which has a significant structural identity to the CBM11 fold and its crystal structure suggests that an individually expressed SdCBM protein could bind agarose like a type B CBM.[36] Additional to the diversity of potential binding properties, MtCBM, CaCBM and FpCBM were chosen due to their origin from thermostable agarases, suggesting thermostable folds, which would be beneficial for applications based on agarose solutions at elevated temperatures, such as 3D printing[6–8] and casting.[17]

To enable direct comparison of the agarose binding capabilities of these four candidate CBMs (sequence data see Table S1), we constructed fusion proteins with the well described and extremely robust esterase 2 (EST2, EC 3.1.1.1)[37] from *Alicyclobacillus acidocaldarius*, an established reporter enzyme,[8,38] which we had previously entrapped in 3D printed agarose hydrogel reactors.[6] All four variants were heterologously expressed and purified from *Escherichia coli* (Figure S1A). Using the previously described spectroscopic assay[6] based on hydrolysis of 5(6)-carboxyfluorescein dihexylester (Figure 1A), we could determine activities ranging from 37% for EST2-CaCBM to 78% for EST2-SdCBM as compared to unmodified EST2 (Figure 1B). To compare the binding efficiency of the fusion proteins to agarose, we subsequently incubated 1 μM of each fusion enzyme and, for control, also unmodified EST2, with a suspension of 2% (w/v) unmelted agarose for 10 min at 25 °C
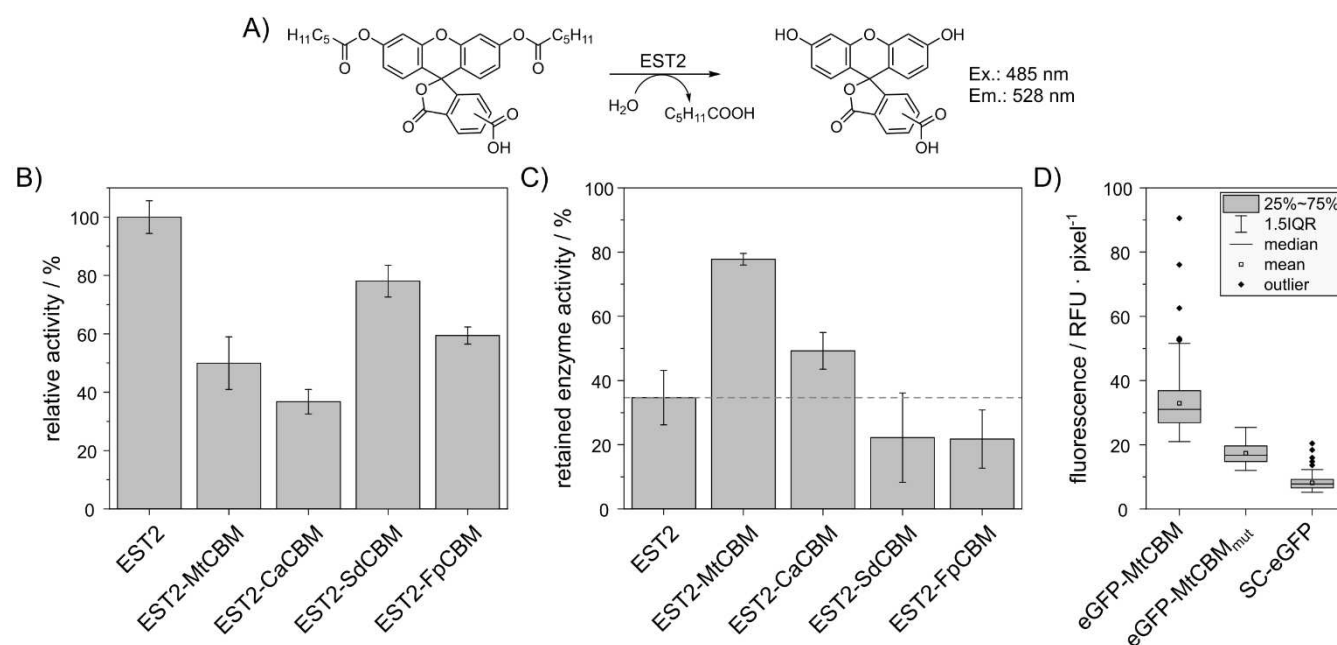

Figure 1. Characterization of EST2 and EST2-CBM fusion enzymes as well as eGFP fusion proteins regarding their agarose-binding capacity. (a) Hydrolytic conversion of the fluorogenic substrate 5(6)-carboxyfluorescein dihexylester due to the enzymatic activity of EST2.[6] (b) Activity of CBM fusion enzymes relative to EST2 with 30 μM substrate in PBS. 100% relative activity corresponds to a turn over number of 69 ± 3 min^{-1}. (c) Amount of EST2 and its CBM fusion enzymes retained by 2% (w/v) unmelted agarose determined by measuring the depletion of a 1 μM enzyme solution. Dotted line indicates 35% of EST2 is retained by agarose. The data is shown as mean values of experimental duplicates with its standard deviation. (d) Using different fusion proteins containing the enhanced fluorescent protein (eGFP), the fluorescence per particle after incubation of eGFP-MtCBM, eGFP-MtCBM$_{mut}$ and SC-eGFP with cross-linked agarose particles and subsequent washing steps was determined. Data for 130 ± 60 particles was analyzed automatically using a python script subtracting background fluorescence and generating a box blot.

ChemCatChem

Research Article
doi.org/10.1002/cctc.202400092

Chemistry Europe
European Chemical
Societies Publishing

and removed the agarose by centrifugal filtration. To avoid bias due to possible changes in enzyme activity caused by agarose binding, we determined the activity of the retained enzyme indirectly based on the reduction of enzymatic activity in the solution (Figure 1C). This analysis showed, that EST2-MtCBM was strongly retained by the agarose with 78% of its activity retained as compared to 35% for unmodified EST2. EST2-CaCBM showed some binding to agarose as indicated by the 49% retained activity. For the SdCBM and FpCBM fusion proteins the retained activities were comparable to EST2, indicating no affinity to agarose under the conditions used here, thus MtCBM was used for all further experiments. The potential effect of agarose binding on enzyme activity was not investigated at this point, as the solid agarose, which was only used for screening purposes, differs considerably from the anticipated hydrogel substrate.

To further confirm that the observed binding was due to a specific interaction of MtCBM and agarose, we exchanged the EST2 enzyme with the enhanced fluorescent protein (eGFP) in the fusion constructs to enable the direct investigation of their binding to commercial cross-linked agarose particles (Work-Beads 40/100 SEC, Bio-Works). In addition to eGFP-MtCBM we also generated a corresponding variant eGFP-MtCBM$_{mut}$, which includes a W94 M point mutation (primer for site-directed mutagenesis see Table S2) resulting in a reduced affinity to oligoagarose in binding site I, as reported for a known mutant of a homologous CBM6.[27] For control purposes, we furthermore generated a SpyCatcher (SC)[39] -modified variant SC-eGFP (40 kDa),[40] which has a similar size to eGFP-MtCBM (44 kDa). All fusions were expressed in *E. coli*, purified (Figure S1B), incubated with a suspension of cross-linked agarose particle and any unbound protein was subsequently washed off. Using a microfluidic observation chip (technical drawings see Figure S2) we were able to quantify the fluorescence per individual agarose particle using a standardized, automated analysis

(Figure S3, exemplary fluorescence microscopy images see Figure S4). As expected, the corresponding analysis of 130 ± 60 particles per fusion protein (Figure 1D) showed a four-fold higher intensity for eGFP-MtCBM when compared to SC-eGFP and twice the intensity of eGFP-MtCBM$_{mut}$. This stronger binding of eGFP-MtCBM$_{mut}$ to the agarose particles compared to the similarly sized SC-eGFP, suggests that although the one-point mutation reduces specific sugar binding, a weak interaction remains via other amino acid residues in the binding pocket. This seems reasonable as the substrate binding mechanism of CBMs, like other sugar-binding proteins,[41] is not only based on CH-π and hydrophobic interactions with aromatic amino acid residues such as W94, but also on additional hydrogen bonds with tyrosine or other polar amino acids.[42] Such an agarose affinity could be based on interactions with a binding site II as reported for other CBM6 s[33–35] or an unspecific affinity of the MtCBM protein due to its surface properties. When comparing the surface properties of MtCBM modeled by AlphaFold2[43] with those of the SC crystal structure (Figure S5), MtCBM displays a distinctly negative patch near the binding site, which could be the reason behind the unexpected sugar binding since residues like arginine, aspartate or glutamate are known to form bidentate interactions with the hydroxy groups of sugars.[44]

Since this analysis confirmed the improved binding of MtCBM and also MtCBM$_{mut}$ fusion proteins to agarose under static conditions, we next investigated their effect on enzyme leaching from agarose hydrogels under flow conditions. To this end, a novel flat-bed agarose (FBA) reactor was designed (Figure 2A, Figure S6), which enables the direct casting of agarose hydrogel films in a reactor bed part with a defined height of 200 μm (Figure S7A), which can then be overflowed with a mobile phase in a cavity with a defined height of 200 μm (Figure S7B). Both the reactor and the later enzyme loading were designed to closely mimic agarose-based flow reactors
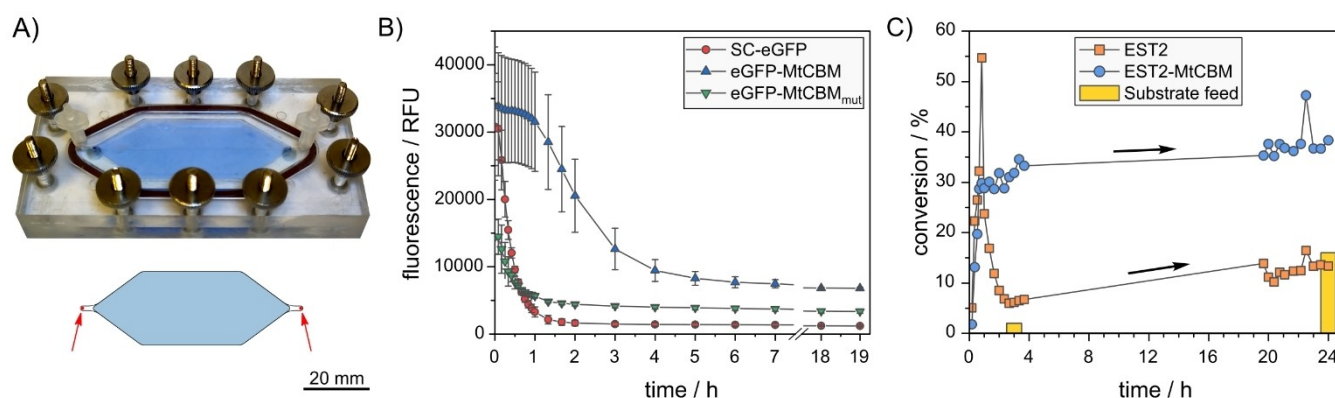

Figure 2. The 200 μm flat-bed agarose (FBA) reactor and initial flow experiment with eGFP- and EST2 fusion proteins. (a) Assembled FBA reactor with agarose hydrogel stained with Royal Blue for visualization and tube adapters connected to the inlet and outlet as well as an overlay of the outlines of the 989 mm² agarose bed (blue) and the reactor room with its inlet and outlet of 1 mm visualized in red. (b) Assessment of agarose-binding of 2 μM SC-eGFP, eGFP-MtCBM and eGFP-MtCBM$_{mut}$ respectively entrapped in 6% agarose #hydrogel under constant perfusion with KP$_i$ 50 mM pH 6.5 at a flow rate of 12.5 μL min⁻¹. The decrease in fluorescence due to leaching was monitored in a 2.5 mm×2.5 mm area in the chip center with a fluorescence microscope (Axio Observer.Z1/7, Carl Zeiss) with $\lambda_{Ex} = 488$ nm and $\lambda_{Em} = 509$ nm under 5x magnification and analyzed using the ZEN Blue software. The data is shown as mean values of experimental duplicates with its standard deviation. (c) Outflow of FBA reactors containing either 2 μM EST2 (orange) or 2 μM EST2-MtCBM (blue) entrapped in 3% agarose hydrogel and perfused with 60 mM 5(6)-carboxyfluorescein dihexylester substrate in PBS at a flow rate of 25 μL min⁻¹. Arrows indicate the increase of conversion caused by spontaneous nonenzymatic hydrolysis of the substrate inside the feed (yellow bars).

ChemCatChem

Research Article
doi.org/10.1002/cctc.202400092

**Chemistry
Europe**

European Chemical
Societies Publishing

used for enzymatic conversions,[6,7,17] allowing for the observation of enzyme leaching and not to achieve a steady-state to ensure a constant product conversion. Typical flow reactors, with non-covalently bound enzymes, achieve such a steady-state condition only when loaded with a sufficient amount of enzyme to prevent enzyme leaching from being observed in conversion curves, a condition attainable even without the use of a binding tag.[6,7] Since this study specifically aimed to examine the efficiency of the enzyme retention and observe changes in conversion, a correspondingly low enzyme loading can be chosen. Moreover, the use of the fluidic FBA reactor, as compared to a batch-based investigation, allows for the examination of complex enzyme systems, such as those with product-induced inactivation, and enables the use of relatively simple fluid dynamic simulations. Three reactors were produced and the depth of the respective reactor bed as well as the height of the resulting agarose hydrogel was determined by laser scanning microscopy and fluorescence microscopy (Table S3). This revealed a reproducible hydrogel height of $143 \pm 10\ \mu m$ that occupies only 77% of the reactor bed part. This deviation can be explained by the literature known gelation-induced contraction and syneresis of agarose and other hydrogels.[45]

FBA reactors were filled with agarose hydrogels containing the three eGFP fusion proteins established above and perfused with potassium phosphate buffer (KP_i) 50 mM pH 6.5 at a flow rate of $12.5\ \mu L\ min^{-1}$. The flush-out of fusion protein was followed by monitoring the mean fluorescence of a $2.5\ mm \times 2.5\ mm$ area in the chip center over a period of 19 h using fluorescence microscopy (Figure 2B). Under these conditions, reactors with eGFP-MtCBM showed a slow initial decrease within the first hour followed by a continuing decrease, until the residual fluorescence stabilized at 20% of the initial fluorescence after 6 h. In contrast, reactors containing eGFP-MtCBM$_{mut}$ and SC-eGFP showed a faster decrease, reaching a stable residual fluorescence after 1.5 h, which was only half (in case of eGFP-MtCBM$_{mut}$) or a quarter (in case of SC-eGFP) of the residual eGFP-MtCBM fluorescence. These results supported the hypothesis that the point mutation W94 M mutation in eGFP-MtCBM$_{mut}$ does not completely eliminate the carbohydrate-binding affinity, since eGFP-MtCBM$_{mut}$ showed a higher residual fluorescence than the similar sized SC-eGFP.

Having confirmed the effect of the MtCBM on the retention of the enzyme in agarose hydrogels, we then investigated this effect in the context of a continuous substrate conversion by the EST2 using the established fluorogenic substrate 5(6)-carboxy-fluorescein dihexylester.[6] To this end, FBA reactors were equipped with 3% agarose hydrogels containing either $2\ \mu M$ EST2 or EST2-MtCBM, and after an initial filling with pure phosphate-buffered saline (PBS) buffer, the FBA reactors were perfused with $60\ \mu M$ 5(6)-carboxyfluorescein dihexylester in PBS buffer. The reactor outflow was sampled at defined timepoints, the reaction was stopped by the addition of guanidinium chloride and the product formation was analyzed spectroscopically with $\lambda_{Ex} = 485\ nm$ and $\lambda_{Em} = 528\ nm$ (Figure 2C). The observed increase in product concentration of both FBA reactor results from the residence time combined with substrate

conversion by the EST2 enzymes. As expected from the binding assessment using the unmelted agarose (Figure 1C), which indicated no affinity to agarose for EST2, the reactor containing the agarose entrapped EST2 exhibited a quick drop in conversion to only 6% within the first two hours, after an initially high conversion of 55%, and thus performed considerably worse than the reactor containing EST2-MtCBM, which showed a constant substrate conversion of 30% within the first four hours after a brief adjustment phase. The initial high conversion can be explained by the higher activity of EST2 compared to EST2-MtCBM (Figure 1B) and an increased contact time of leached EST2 with substrate in the dead volume between reactor outlet and sampling into the stop solution. Surprisingly, both reactors showed a continuous increase in substrate conversion over time, which was more pronounced in the EST2-containing reactor. This increase was likely caused by the well-known spontaneous hydrolysis of fluorescein diesters.[46] As expected the 5(6)-carboxyfluorescein dihexylester substrate indeed also hydrolyzes inside the substrate feed with a spontaneous nonenzymatic conversion of 2% within 3 h and 16% within 24 h when incubated in a closed reaction tube (Figure 2C, yellow bars). This spontaneous hydrolysis follows pseudo-first-order reaction kinetics without reaching a steady state, which leads to a constantly increasing concentration of the hydrolyzed substrate in the feed. As the enzymatic activity in the reactor decreases at the same time, the non-enzymatic process becomes "dominant". Taking this effect into account, we determined a corrected conversion after 24 h of 0% for the reactor containing EST2 and 21% for the EST2-MtCBM reactor.

Next we expanded the scope of application of the MtCBM to the cofactor-free phenacrylate decarboxylase also referred to as phenolic acid decarboxylase (PAD, EC 4.1.1.102)[47,48] from *Enterobacter* spec. that has previously also been entrapped successfully in 3D printed agarose hydrogels reactors.[7] Importantly, the substrate of the enzyme reaction *p*-coumaric acid (Figure 3A) is stable and not prone to nonenzymatic decarboxylation. Moreover, the reverse carboxylation of the product is negligible, as it can only be observed in the presence of extremely high hydroxycarbonate concentrations.[49] Therefore, the fusion enzymes PAD-MtCBM as well as PAD-MtCBM$_{mut}$ were generated (sequence data see Table S1) and after expression in *E. coli* and purification along with PAD[7] and PAD-SC[50] (Figure S1C), we determined their activity with *p*-coumaric acid as described previously.[7] Our findings revealed that the enzymatic activities across all enzymes were within a comparable range, with only a slightly elevated activity observed for the fusion enzymes (Figure 3B). Interestingly, the fusion of MtCBM to the PAD enzyme did not decrease the activity as it did when fused to EST2 (Figure 1B).

To gain further insights into MtCBM binding, we determined the K_D of PAD-MtCBM and PAD-MtCBM$_{mut}$ with oligomeric neoagarohexaose (6NA) using isothermal titration calorimetry (ITC). 6NA is a hexameric agarose with 3,6-anhydrogalactose at the non-reducing end. To this end, we titrated 1.25 mM of 6NA into $200\ \mu M$ enzyme and measured the occurring temperature change using a MicroCal PEAQ-ITC (Malvern Panalytical). As expected from the literature,[27] this experiment revealed that
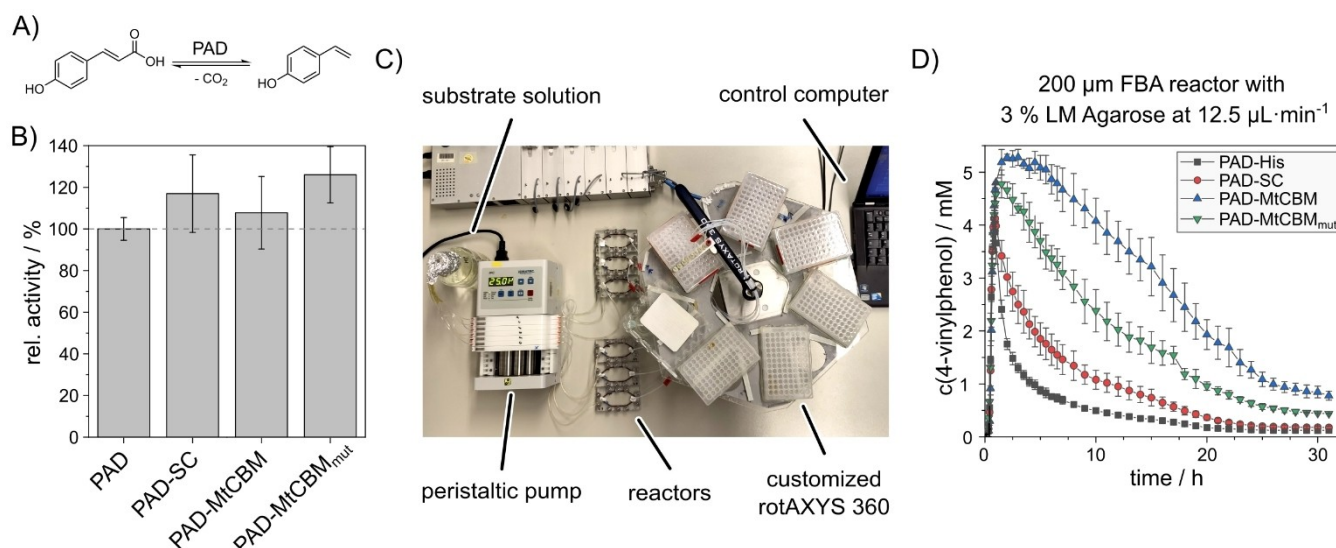
ChemCatChem

Research Article
doi.org/10.1002/cctc.202400092

Chemistry Europe
European Chemical
Societies Publishing

Figure 3. Characterization of PAD and its fusion enzymes and flow experiment with PAD fusion enzymes in FBA reactors. (a) Decarboxylation of *p*-coumaric acid into 4-vinylphenol catalyzed by PAD used for determining the enzymatic activity. (b) Activity of PAD and its fusion enzymes relative to PAD with 0.125 mM *p*-coumaric acid as determined earlier.[7] Dotted line indicates the 100% activity of PAD. Analyses was carried out in experimental duplicates. (c) Setup for flow experiments with six parallel FBA reactors utilizing a peristaltic pump in combination with a customized rotAXYS 360 positioning system (cetoni) for fraction collection. (d) Concentration of 4-vinylphenol in the outflow of the FBA reactors equipped with PAD, PAD-SC, PAD-MtCBM and PAD-MtCBM$_{mut}$ in 3% agarose hydrogel at a flow rate of 12.5 μL min^{-1} quantified by RP–HPLC. Reaction condition: 5 mM *p*-coumaric acid in KP$_i$ 50 mM pH 6.5 at room temperature. The data is shown as mean values of at least experimental duplicates with its standard deviation.

PAD-MtCBM$_{mut}$ did not bind 6NA while PAD-MtCBM showed an K$_D$ of $2.4 \pm 0.1 \times 10^{-5}$ M (Figure S8), which is in the same range as K$_D$ of other reported CBM6s.[27,51] Moreover, MtCBM showed a 10-fold stronger binding than the previously reported agarose-binding tag derived from *L. sulphureus* with a K$_D$ of only 1.7×10^{-4} M.[25] ITC was also employed to evaluate the long-term stability of PAD-MtCBM and its interaction with 6NA, which showed no significant changes upon incubation for up to 42 h (Figure S9A). Additionally, the activity of PAD fusion enzymes showed a maximum reduction of only 10% after 22 h, regardless of whether they were incubated in homogeneous solution or integrated into agarose hydrogel bricks, prepared as previously described[6] (Figure S9B). Thus, all fusion proteins were suitable for applications in flow experiments for at least two days.

After initial filling with in KP$_i$ 50 mM pH 6.5, FBA reactors equipped with 2 μM PAD fusion enzymes entrapped in 3% agarose hydrogel were perfused with 5 mM *p*-coumaric acid in KP$_i$ 50 mM pH 6.5. In order to realize a parallelization and automatization of six flow reactors, a set-up with a peristaltic pump in combination with a customized rotAXYS 360 positioning system (cetoni) for fractionation of the reactor outflow was used (Figure 3C). At defined time intervals, 75 μL of the outflow were collected into 225 μL of a 2:1-mixture of propylene glycol with aqueous 0.1% trifluoroacetic acid supplemented with 1 M cinnamic acid as internal standard, diluted 1:1 in acetonitrile and analyzed by reverse-phase HPLC (Figure S10). In accordance with previous PAD flow experiments[7] a flow rate of 12.5 μL min^{-1} was applied. Under these reaction conditions, as expected from the previous FBA reactor experiments with EST2 and eGFP fusion proteins (Figure 2B and C), FBA reactors containing PAD and PAD-SC showed an initial high conversion

followed by a fast decrease. In contrast, the PAD-MtCBM containing reactor showed an initial conversion of over 90% within the first 6 h followed by a slow decrease over several hours (Figure 3D). We also analyzed the outflows of the FBA reactor using western blot analysis, which showed detectable amounts of protein only in the outflow of PAD and PAD-SC containing reactors (Figure S11). While the faster decrease in substrate conversion for the PAD (20 kDa) containing reactor can be explained by a faster leaching due to its smaller size than PAD-SC (33 kDa), the markedly slower decrease for PAD-MtCBM$_{mut}$ (36 kDa) compared to PAD-SC cannot be explained solely by the 10% increased protein size, again indicating a residual affinity for agarose as described above.

Since the retention of enzymes can also be influenced by modulating the hydrogel thickness, FBA reactors with increased depths of the hydrogel containing reactor bed part of 400 μm and 600 μm were fabricated (compare Figure S7A). In order to minimize the influence of the volume of the mobile phase above the hydrogel, we kept the height of the cavity in the reactor above the hydrogel unchanged at 200 μm (see Figure S7B). The new reactor bed parts as well as the respective hydrogels were characterized by laser scanning microscopy and fluorescence microscopy as before (Table S3). Again, fluorescence microscopy measurements of the cast hydrogels showed that they occupied only 74% and 73% of the reactor bed part, respectively, which is consistent with the 77% determined for the 200 μm FBA reactor. Due to this gelation-induced contraction the heights of the mobile phase containing spaces over the hydrogel is also changing from 253 ± 9 μm in the 200 μm FBA reactors to 309 ± 4 μm and 364 ± 2 μm in the 400 μm and 600 μm FBA reactors.

We furthermore investigated the effect of an increased agarose concentration of 6% on enzyme retention, thus, all three FBA reactor variants (200 µm, 400 µm, and 600 µm) were filled with agarose hydrogels (6%) incorporating PAD fusion enzymes at concentrations of 2 µM, 1 µM, and 0.67 µM, respectively. This approach was employed to ensure a consistent total enzyme load across the reactors independent of the hydrogel volume. As before, after initial filling with in KPi 50 mM pH 6.5 the hydrogels were perfused with 5 mM p-coumaric acid in KP$_i$ 50 mM pH 6.5 at a flow rate of 12.5 µL min^{-1} (Figure 4 A, Figure S12A and B). These experiments revealed that in the 200 µm FBA reactor with 6% agarose (Figure 4A) only PAD-MtCBM showed a higher conversion over time when compared to the 3% agarose reactor (Figure 3D), while the retention of similarly sized PAD-SC and PAD-MtCBM$_{mut}$ was not influenced by the higher agarose concentration. This excludes an improved entrapment due to pore size reduction with increasing agarose concentration, which would increase retention of all three enzymes and is also in line with literature reports, indicating that the pore size reduction stagnates for agarose concentrations higher than 3%.[52,53] Moreover, the pore sizes of agarose hydrogels reported in literature (289±66 nm in 3% agarose and 201±36 nm in 5% agarose hydrogels)[53] are orders of magnitude larger than those of the PAD fusion enzymes evaluated in this study. For instance, a model of the structure of PAD-SC exhibits dimensions of 9.1 nm×7.7 nm ×4.6 nm (Figure S13). The increased retention of PAD-MtCBM, can thus be explained by an increased number of agarose binding sites for MtCBM due to the higher amount of agarose per volume. The influence of the different hydrogel heights (Figure 4A, S12 A and B) revealed that only the reactors containing PAD-SC and PAD-MtCBM$_{mut}$ profited from an increased thickness, while the performance of the PAD-MtCBM-containing reactors were not influenced. This is further illustrated by calculating the total quantity of product produced within 30 h (Figure 4B, see data for 10 h and 20 h in Figure S12C and D). The results suggest that the reactors containing PAD-SC and PAD-MtCBM$_{mut}$ can benefit from longer diffusions lengths and therefore an improved retention, while for PAD-MtCBM the desorption from the agarose matrix is the rate-determining step. Furthermore, it is evident that even tripling the hydrogel height is not sufficient to increase the retention of PAD-SC in FBA reactors to a degree that matches the performance of PAD-MtCBM-containing reactors (Figure 4B).

We further determined the influence of different flow rates by perfusing the 200 µm FBA reactor containing 2 µM PAD-SC, PAD-MtCBM or PAD-MtCBM$_{mut}$ with 5 mM p-coumaric acid at a flow rate of 12.5, 25 and 100 µL min^{-1} (Figures 4A, 5A and S14A). While increasing the flow rate to 25 µL min^{-1} led to only minor changes in conversion within the first 10 h for all fusion enzymes when compared to the behavior at 12.5 µL min^{-1}, the conversion after 31 h in the reactor containing PAD-MtCBM dropped to 0.8±0.1 µM at 25 µL min^{-1} (Figure 5A) as compared to the 1.8±0.1 µM for 12.5 µL min^{-1} (Figure 4A). Since doubling the flow rate did not show any noticeable impact on the time-dependent decrease in conversion of the physically entrapped PAD-SC the influence of the flow rate on enzyme leakage was considered to be neglectable. When the flow rate was further increased to 100 µL min^{-1} (Figure S14A), none of the reactors reached full conversion (5 mM) due to the reduced dwell time, however, the overall trend remained the same with PAD-MtCBM showing the highest conversions. However, since the time-dependent conversion of the PAD-MtCBM$_{mut}$-containing FBA reactor exhibits increased standard deviation (Figure S14A, green curve), we focused on the interpretation of the FBA reactors containing PAD-SC and PAD-MtCBM. For instance, the data reliably suggests that the same amount of PAD-MtCBM catalyst produced three times of the total amount of product
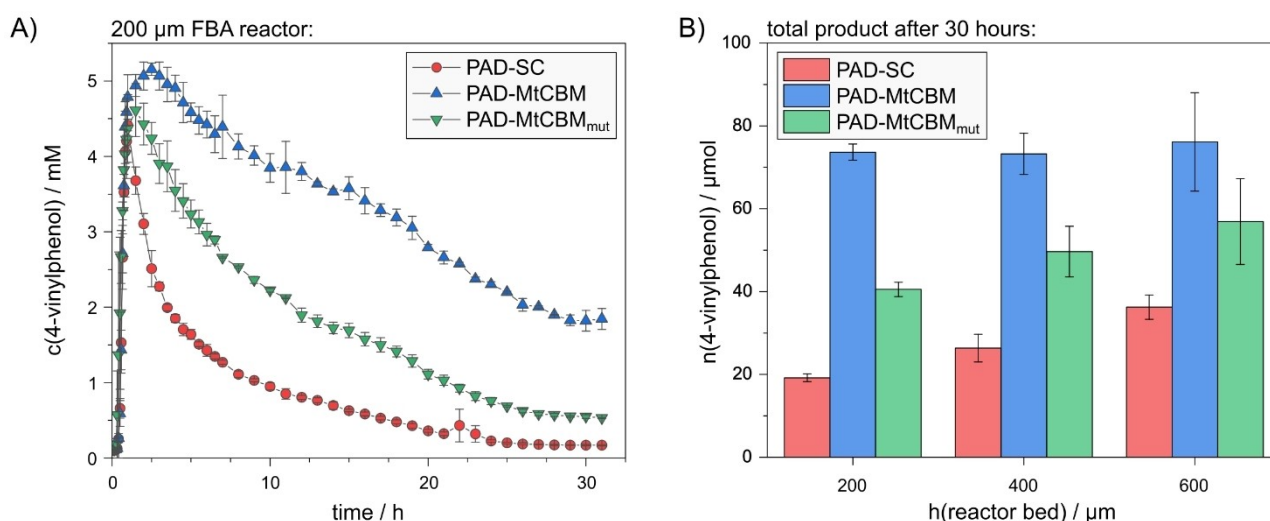

Figure 4. Flow experiments with different reactor bed heights regarding the conversion by similarly sized fusion enzymes PAD-SC (33 kDa, red), PAD-MtCBM (36 kDa, blue), and PAD-MtCBM$_{mut}$ (36 kDa, green) in FBA reactors. (a) Performance of 200 µm FBA reactors, as well as (b) total amount of 4-vinylphenol generated by FBA reactors with reactor beds of 200 µm, 400 µm and 600 µm after 30 h. 6% agarose hydrogels containing the enzymes were perfused with 5 mM p–coumaric acid in KP$_i$ 50 mM pH 6.5 at room temperature and a flow rate of 12.5 µL min^{-1}. The effluent quantified by HPLC. The resulting enzyme concentration in the hydrogel were 2 µM (200 µm), 1 µM (400 µm) and 0.67 µM (600 µm) keeping the enzyme amount in the reactor identical. The data is shown as mean values of at least experimental duplicates with its standard deviation.
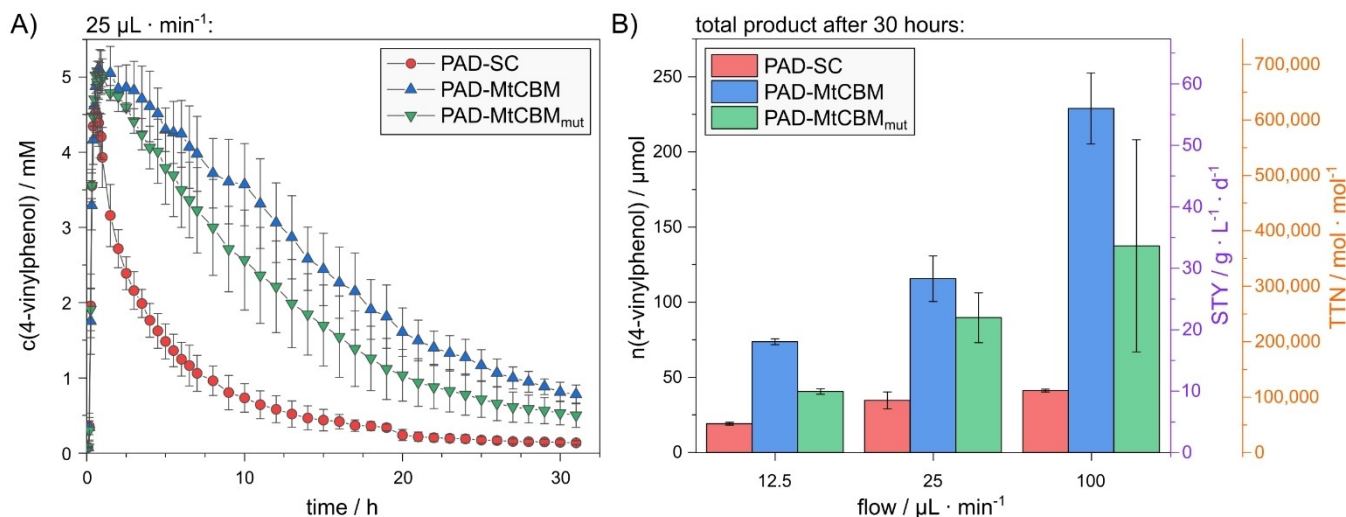
ChemCatChem

Research Article
doi.org/10.1002/cctc.202400092

Chemistry
Europe
European Chemical
Societies Publishing

Figure 5. Flow experiments with different flow rates regarding the conversion by similarly sized fusion enzymes PAD-SC (33 kDa, red), PAD-MtCBM (36 kDa, blue), and PAD-MtCBM$_{mut}$ (36 kDa, green) in FBA reactors. (a) Reactor performance of 200 µm FBA reactors perfused with different flow rate of 25 µL min^{-1}, and (b) total amount of 4-vinylphenol generated by FBA reactors perfused with flow rates of 12.5, 25 and 100 µL min^{-1} after 30 h as well as their space-time yield (STY, purple axis) and total turnover number (TTN, orange axis). 2 µM enzyme in 6% agarose hydrogels were perfused with 5 mM *p*-coumaric acid in KP$_i$ 50 mM pH 6.5 at room temperature and the effluent quantified by HPLC. The data is shown as mean values of at least experimental duplicates with its standard deviation.

after 30 h when comparing the lowest and the highest flow rate indicating a better utilization of the catalyst under such conditions (Figure 5B, see data for 10 h and 20 h in Figure S14B and C). This also enabled us to evaluate the effectiveness of PAD-MtCBM in the 200 µm FBA reactor after 30 h revealing a maximum space-time yield of 56 ± 4 g L^{-1} d^{-1} and total turnover number of $622,000 \pm 46,000$, which is 6-fold higher than with PAD-SC (Figure 5B).

To acquire a better understanding of the system, we aimed to simulate the performance of the FBA reactors using the COMSOL Multiphysics software. Apart from the already obtained data, we experimentally determined additional parameters for the simulation. First, we investigated the amount of enzyme inside the agarose hydrogel that is not bound to the agarose matrix and can thus be washed out immediately. To this end, bricks were casted from agarose containing either 2 µM PAD-SC, PAD-MtCBM or PAD-MtCBM$_{mut}$ in KP$_i$ 50 mM pH 6.5. The liquid phase was separated from the agarose matrix via centrifugal filtration combined with mechanical disruption, and the amount of unbound enzyme in the liquid phase was determined by the enzymatic activity found in the respective fractions (Figure S15). This indicated that 79% of PAD-SC and 10% of PAD-MtCBM$_{mut}$ were not bound by agarose, while for PAD-MtCBM only 2% were free in solution. In order to further support this finding, we performed an additional western blot analysis of the liquid phase (Figure S16A and B). This revealed that 89% of PAD-SC and 13% of PAD-MtCBM$_{mut}$ were not bound by agarose, while the unbound amount of PAD-MtCBM could not been detected. Considering that the limit of detection in this western blot analysis is 0.04 µM of enzyme, we assumed this concentration for unbound PAD-MtCBM. Furthermore, this allow use the assessment of the effectiveness of enzyme binding to agarose matrix revealing that PAD-MtCBM exhibits

an immobilization yield of at least 98% (Figure S16C). As the FBA reactor system does not reach steady-state conditions, this characterization can only be achieved prior to setting up a flow reactor. Furthermore, we determined the inhibition of PAD enzymes by the reaction product 4-vinylphenol, as reported for homologous enzymes.[53,55,56] The underlying relation of K_i to K_m in the apparent K_m for the competitive product inhibition of PAD-SC, PAD-MtCBM and PAD-MtCBM$_{mut}$ was measured by the decrease in activity in the presence of increasing amounts of product. Following a previously described procedure (Equation S1 and S2),[55] the activity decreases could be fitted by regression of K_m and K_i (Figure S17A, C, E).

With these results at hand, we were able (for a detailed discussion, see Figure S17) to describe the relation of K_i to K_m through second-degree polynomial functions (Figure S17B, D, F). We then characterized PAD-SC, PAD-MtCBM and PAD-MtCBM$_{mut}$ analyzing the reaction kinetics and determining their Michaelis-Menten parameters across a range of *p*-coumaric acid concentrations from 0.2 to 5.5 mM. In order to obtain the parameters, calculated progression curves of the conversion (Equation S3 and S4) were fitted to the measured product production by minimizing the sum of squared deviations (Figure S18). The resulting K_m values, ranging from 2.3 to 3.4 mM, were comparable to the previously reported K_m of 2.2 for the same enzyme with a different substrate,[48] while the obtained k_{cat} values of 224–266 s^{-1} were about 100-times higher. This is not surprising since it has been reported that the maximum velocities of PADs are more divers than their K_m values.[55] The K_i values of 0.33 mM, 0.23 mM and 0.28 mM for PAD-SC, PAD-MtCBM and PAD-MtCBM$_{mut}$, respectively, are again in the same order of magnitude as previously reported constants.[54,55] In addition to the Michaelis-Menten parameters, we also determined possible 4-vinylphenol-dependent enzyme

ChemCatChem

Research Article
doi.org/10.1002/cctc.202400092

**Chemistry
Europe**
European Chemical
Societies Publishing

inactivation rates (k_{in}). To this end, PAD-SC, PAD-MtCBM or PAD-MtCBM$_{mut}$ were incubated with 0.5–5 mM 4-vinylphenol and the residual enzyme activity was measured after 8 min, 2 h and 8 h of incubation. From the resulting inactivation curves, we could then calculate k_{in} for all three enzymes (Figure S19). Since k_{in} was comparable for all PAD fusions, we decided to use the mean value of $4.7 \pm 2.7 \times 10^{-6}$ s^{-1} mM^{-1} for the simulation.

When performing the reactor simulation using the COMSOL Multiphysics 6.1 software, a laminar flow over a porous medium (hydrogel) was assumed. Due to the symmetry of the FBA reactors, the required computational effort could be reduced by choosing a reactor model that represents only one half of the reactor (Figure S20A) based on the experimentally determined dimensions of the reactor parts, the hydrogel and the cavity above the hydrogel (Table S3). Coupled mass transfer phenomena and enzymatic reactions including inhibition and inactivation were calculated using finite element modeling (FEM) with a mesh size of 10–50 µm (Figure S20B). In addition to the enzyme parameters (K_m, k_{cat}, K_i and k_{in}) determined above, diffusion coefficients derived from literature were included. A diffusion coefficient of 1.2×10^{-10} m$^2 \cdot$s^{-1} was chosen for substrate and product due to previously measured diffusion of another small molecule inside 6% agarose hydogels[8] and 10^{-11} m^2 s^{-1} for enzyme diffusion based on the diffusion of lysozyme inside agarose[57] (for a list of all enzyme-specific parameters, see Tables S4–S6). The enzyme-specific desorption rate (k_{des}) of the agarose-bound enzymes was implemented by a second order kinetics (Equation S5). Using the experimentally determined product concentrations of the 200 µm FBA reactor experiments at a flow rate of 25 µL min^{-1} (Figure S5A), k_{des} values of 4×10^{-4} s^{-1}, 0.5×10^{-4} s^{-1} and 2×10^{-4} s^{-1} could be approximated for PAD-SC, PAD-MtCBM and PAD-MtCBM$_{mut}$, respectively. The results showed the expected stronger agarose binding of the MtCBM protein, which could have not been determined in a batch experiment. These k_{des} values determined were then transferred to all other simulation runs without further adjustment and were applied together with the other model parameters (Table S4–S6) for all flow experiments with different hydrogel heights (Figure 4) and flow rates (Figure 5) resulting in simulations of product concentrations in the effluent (Figure S21, see distribution of product and substrate within FBA reactors in Figure S22).

The predicted product concentrations as well as the respective total amount of product generated after 30 h (Figure 6, striped bars) agreed quite well with the experimental results in all flow experiments. Especially the simulated data of flow experiments at 12.5 µL min^{-1} and different hydrogel heights (Figure 6A) was in good accordance to the experimental data, with only larger deviations obtained from the 200 µm FBA reactor experiment with PAD-MtCBM$_{mut}$ (Figure 6A, green bars). In order to assess influence of mass transfer resistance on the reactor performance, the local effectiveness factor (η) was calculated from the dimensionless Thiele modulus as described previously but with additional competitive product inhibition (Figure S23).[12] The effectiveness factor relates the reduced reaction rate of the enzyme in the hydrogel to that of the free enzyme under the same conditions. When comparing η over different hydrogel heights (Figure S23A), it becomes clear that the effectiveness factor η decreases with increasing height of the hydrogel. Conversely, when comparing η over different time points (Figure S23B), it becomes clear that η increases with time. This is due to the fact that the parameters for mass transport remain constant, but the reaction rate itself decreases due to enzyme leaching and product-induced enzyme inactivation.

Differences between the simulated and experimental results could also be seen in the 200 µm FBA reactor experiments with flow rates of 100 µL min^{-1} (Figure 6B), where the model
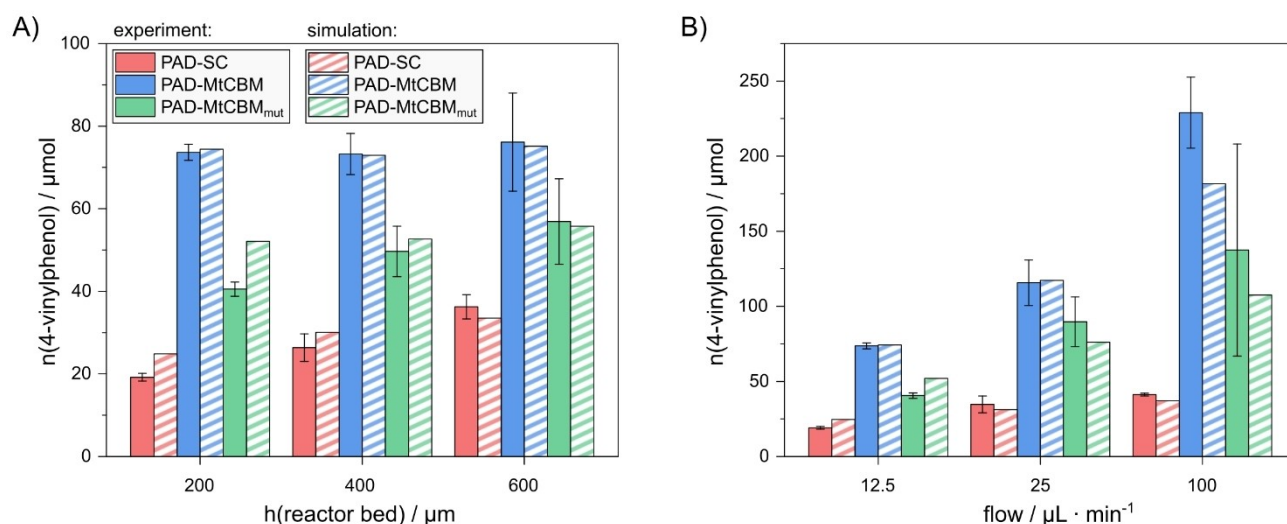

Figure 6. Total amount of product generated after 30 h of FBA reactors with (a) different hydrogel heights and (b) different flow rates based on experimental (solid bars) and simulated data (striped bars) for FBA reactors containing 6% agarose hydrogel with PAD-SC (red), PAD-MtCBM (blue) and PAD-MtCBM$_{mut}$ (green). The experimental data is shown as mean values of at least experimental duplicates with its standard deviation and identical with Figure 4B and Figure 5B. The simulated data was generated by integrating the reactor performance curves in Figure S21. FBA reactors with 200 µm, 400 µm, and 600 µm reactor beds were perfused with 12.5 µL min^{-1} and 200 µm FBA reactors perfused with flow rates of 25 µL min^{-1} and 100 µL min^{-1}.

predicted lower conversion for PAD-MtCBM (Figure 6B, blue bars) and PAD-MtCBM$_{mut}$ (Figure 6B, green bars). These observations indicated that the model's capacity to replicate the behavior for PAD-MtCBM and PAD-MtCBM$_{mut}$ was limited when using high flow rates. Still, the simulation suggests that the primary determinant contributing to the decline in reactor performance is the loss of the enzyme, as opposed to product-induced enzyme inactivation. As the difference in productivity is smallest within the first 10 h for PAD-SC and PAD-MtCBM in the 600 μm FBA reactor (Figure S12C), the effects of enzyme leakage and inactivation were considered in more detail for this period (Figure S24). As expected, it is clear that the reduced performance of the predominantly physically entrapped PAD-SC is due to enzyme loss by diffusion from the hydrogel, with the initial amount of enzyme halved after 2 h (Figure S24A). Conversely and as expected, the rate-limiting step for leaching of PAD-MtCBM is desorption from the agarose matrix. Approximately 85% of the enzyme remains within the hydrogel after 2 h and this decreases to 40% after 10 h. However, product-induced enzyme inactivation also significantly affects PAD-MtCBM, resulting in approximately 50% of the remaining enzyme being inactivated after 10 h (Figure S24B). The obtained k_{des} values further suggest that, despite PAD-MtCBM$_{mut}$ initially exhibiting a higher enzyme binding capacity to the agarose matrix, its desorption rate falls within the same range as PAD-SC. Thus, the W94 M mutation effectively eliminates specific agarose binding, resulting in only weak nonspecific affinity to agarose.

Conclusions

In conclusion, we herein demonstrated that the MtCBM derived from a thermostable agarose, can be utilized as an efficient binding tag in fusion proteins that can increase the retention of various enzymes in agarose hydrogels under flow conditions. MtCBM displayed a high affinity towards unmelted agarose when fused to the reporter enzyme EST2 or the fluorescent protein eGFP. Using a novel flat-bed agarose reactor that allowed to compare agarose hydrogels of defined thickness and volume under defined flow conditions as well as defined contact area of liquid phase and hydrogel, we could show an increased retention for fusion proteins of MtCBM with eGFP as well as the enzymes EST2 and PAD. Determination of the affinity of PAD-MtCBM to neoagarohexaose via ITC revealed a K_D of $2.4 \pm 0.1 \times 10^{-5}$ M which is higher than other previously reported purification tags based on agarose binding.[25]

We also showed, that the protein PAD-MtCBM$_{mut}$, carrying the mutation W94 M previously reported for a homolog CBM6,[27] could indeed eliminate the specific binding of PAD-MtCBM$_{mut}$ to oligoagarose. However, MtCBM$_{mut}$ displays a remaining affinity for agarose hydrogels and crosslinked agarose particles. Utilizing the ability to precisely control reactor parameters in the novel FBA reactor such as hydrogel thickness, flow rate, agarose concentration, initial enzyme loading and via experimental determination of K_m, K_i, k_{cat}, k_{in}, and activity loss during hydrogel casting we could approximate desorption rate

values k_{des} via simulation. We could show that the better performance of the FBA reactors containing PAD-MtCBM during prolonged flow reactions is mainly caused by a reduced desorption from the agarose matrix as compared to the similar sized PAD-SC. However, no steady-state conditions could be achieved by employing the MtCBM modification due to effects such as product-induced inactivation of the enzyme. We demonstrated that, despite tripling the hydrogel height from 200 μm to 600 μm, the retention of PAD-SC is insufficient to achieve a comparable total substrate conversion as observed for PAD-MtCBM immobilized in a 200 μm hydrogel. Although further increase in the hydrogel height might result in a comparable total substrate conversion for PAD-SC, this would have the drawback of imposing higher mass transfer limitations due to elongated diffusion lengths.[9,10] To further enhance the performance of the FBA reactors real-time analytics[58] or mathematical models[59] combined with automatically adjustment of reaction conditions, as shown by Claaßen et al. in a batch approach,[60] could be employed. Furthermore, implementation of liquid–liquid extractions along with feedback loop strategies could further increase yields by recycling remaining substrate in the outflow back to the reactor.[61]

This shows that the MtCBM as a genetically encoded fusion tag is an elegant solution to increase enzyme retention in agarose hydrogels, without a need for chemical or reactor geometry modification. The MtCBM evaluated in this work has further potential applications also in reactor formats such as 3D-printed agarose hydrogels and packed-bed formats since it also binds to crosslinked agarose particles as well as unmelted agarose. Potential applications should not be limited to carbohydrates, as it was shown that for example CBM4 from *Clostridium thermocellum* was capable of bind and modify carbon nanotubes, and other CBMs were engineered towards metal-binding or PET-binding properties.[62] Based on these finding, we believe that the MtCBM protein is not only a powerful tag to increase the immobilization stability of enzymes in agarose hydrogels but also has great potential for further applications involving protein binding.

Experimental Section

Experimental details can be found in the Supporting Information.

Supporting Information

The authors have cited additional references within the Supporting Information.[63] Symbols and their definitions used in this study are provided in the Supporting Information (Table S7).

ChemCatChem

Research Article
doi.org/10.1002/cctc.202400092

Chemistry
Europe
European Chemical
Societies Publishing

Conflict of Interests

The authors declare no conflict of interest.

Data Availability Statement

The data that support the findings of this study are available from the corresponding author upon reasonable request.

[1] a) C. M. Heckmann, F. Paradisi, *ChemCatChem* **2020**, *12*, 6082; b) S. Wu, R. Snajdrova, J. C. Moore, K. Baldenius, U. T. Bornscheuer, *Angew. Chem. Int. Ed.* **2020**, *60*, 88; c) L. Leemans Martin, T. Peschke, F. Venturoni, S. Mostarda, *Curr. Opin. Green Sustain. Chem.* **2020**, *25*, 100350; d) S. Simić, E. Zukić, L. Schmermund, K. Faber, C. K. Winkler, W. Kroutil, *Chem. Rev.* **2021**, *122*, 1052; e) R. Buller, S. Lutz, R. J. Kazlauskas, R. Snajdrova, J. C. Moore, U. T. Bornscheuer, *Science (N. Y.)* **2023**, *382*, eadh8615.

[2] E. L. Bell, W. Finnigan, S. P. France, A. P. Green, M. A. Hayes, L. J. Hepworth, S. L. Lovelock, H. Niikura, S. Osuna, E. Romero et al., *Nat. Rev. Methods Primers* **2021**, *1*, 46.

[3] a) R. K. Singh, M. K. Tiwari, R. Singh, J.-K. Lee, *Int. J. Mol. Sci.* **2013**, *14*, 1232; b) A. Basso, S. Serban, *Mol. Catal.* **2019**, *479*, 110607; c) K. S. Rabe, J. Müller, M. Skoupi, C. M. Niemeyer, *Angew. Chem. Int. Ed.* **2017**, *56*, 13574; d) P. Žnidaršič-Plazl, *Curr. Opin. Green Sustain. Chem.* **2021**, *32*, 100546; e) M. Santi, L. Sancineto, V. Nascimento, J. Braun Azeredo, E. V. M. Orozco, L. H. Andrade, H. Gröger, C. Santi, *Int. J. Mol. Sci.* **2021**, *22*, 990; f) A. Naramittanakul, S. Buttranon, A. Petchsuk, P. Chaiyen, N. Weeranoppanant, *React. Chem. Eng.* **2021**, *6*, 1771.

[4] M. Romero-Fernández, F. Paradisi, in *Catalyst Immobilization. Methods and Applications* (Eds: M. Benaglia, A. Puglisi), Wiley-VCH, Weinheim **2020**, 409–435.

[5] J. Meyer, L.-E. Meyer, S. Kara, *Eng. Life Sci.* **2022**, *22*, 165.

[6] M. Maier, C. P. Radtke, J. Hubbuch, C. M. Niemeyer, K. S. Rabe, *Angew. Chem. Int. Ed.* **2018**, *57*, 5539.

[7] M. Peng, E. Mittmann, L. Wenger, J. Hubbuch, M. K. M. Engqvist, C. M. Niemeyer, K. S. Rabe, *Chem. Eur. J.* **2019**, *25*, 15998.

[8] L. Wenger, C. P. Radtke, E. Gerisch, M. Kollmann, C. M. Niemeyer, K. S. Rabe, J. Hubbuch, *Front. Bioeng. Biotechnol.* **2022**, *10*, 928878.

[9] B. Schmieg, J. Döbber, F. Kirschhöfer, M. Pohl, M. Franzreb, *Front. Bioeng. Biotechnol.* **2019**, *6*, 211.

[10] R. A. Sheldon, S. van Pelt, *Chem. Soc. Rev.* **2013**, *42*, 6223.

[11] a) L.-E. Meyer, D. Horváth, S. Vaupel, J. Meyer, M. Alcalde, S. Kara, *React. Chem. Eng.* **2023**, *8*, 984; b) M. Nöth, E. Gau, F. Jung, M. D. Davari, I. El-Awaad, A. Pich, U. Schwaneberg, *Green Chem.* **2020**, *22*, 8183; c) N. C. Dubey, D. Gaur, B. P. Tripathi, *J. Polym. Sci.* **2023**, *61*, 1730.

[12] B. Schmieg, M. Nguyen, M. Franzreb, *Front. Bioeng. Biotechnol.* **2020**, *8*, 365.

[13] E. Gkantzou, M. Weinhart, S. Kara, *RSC Sustain.* **2023**, *1*, 1672.

[14] W. Y. Zhang, W. Zhang, Z. Liu, C. Li, Z. Zhu, C. J. Yang, *Anal. Chem.* **2012**, *84*, 350.

[15] U. N. Lee, J. H. Day, A. J. Haack, R. C. Bretherton, W. Lu, C. A. DeForest, A. B. Theberge, E. Berthier, *Lab Chip* **2020**, *20*, 525.

[16] H.-J. Kim, D. J. Min, S. H. Lee, J. W. Lim, N. Jung, H. W. Ryu, J. H. Jeong, *Mater. Lett.* **2019**, *253*, 298.

[17] F. Croci, J. Vilím, T. Adamopoulou, V. Tseliou, P. J. Schoenmakers, T. Knaus, F. G. Mutti, *ChemBioChem* **2022**, *23*, e202200549.

[18] a) M. Ali, Q. Husain, *Int. J. Biol. Macromol.* **2018**, *116*, 463; b) H.-J. Kong, K. Y. Lee, D. J. Mooney, *Polymer* **2002**, *43*, 6239; c) N. Zhang, J. Wang, J. Ye, P. Zhao, M. Xiao, *Int. J. Biol. Macromol.* **2018**, *117*, 696; d) Q. Xiao, H. Weng, G. Chen, A. Xiao, *Food Chem.* **2019**, *279*, 30; e) T. Menegatti, P. Žnidaršič-Plazl, *Front. Bioeng. Biotechnol.* **2021**, *9*, 752064; f) A. Awadhiya, D. Kumar, V. Verma, *Carbohydr. Polym.* **2016**, *151*, 60; g) K. Firipis, M. Boyd-Moss, B. Long, C. Dekiwadia, W. Hoskin, E. Pirogova, D. R. Nisbet, R. M. I. Kapsa, A. F. Quigley, R. J. Williams, *ACS Biomater. Sci. Eng.* **2021**, *7*, 3340; h) X. Qi, X. Su, X. Tong, W. Xiong, Q. Zeng, Y. Qian, Z. Zhou, X. Wu, Z. Li, L. Shen et al., *Carbohydr. Polym.* **2019**, *224*, 115208.

[19] A. I. Freitas, L. Domingues, T. Q. Aguiar, *J. Adv. Res.* **2022**, *36*, 249.

[20] a) S. Chong, F. B. Mersha, D. G. Comb, M. E. Scott, D. Landry, L. M. Vence, F. B. Perler, J. Benner, R. B. Kucera, C. A. Hirvonen, et al., *Gene* **1997**, *192*, 271; b) M. Q. Xu, H. Paulus, S. Chong, *Methods Enzymol.* **2000**, *326*, 376; c) S. F. Mitchell, J. R. Lorsch, *Methods Enzymol.* **2015**, *559*, 111.

[21] a) H. Bedouelle, P. Duplay, *Eur. J. Biochem.* **1988**, *171*, 541; b) C. Di Guan, P. Li, P. D. Riggs, H. Inouye, *Gene* **1988**, *67*, 21.

[22] M. X. van Bemmelen, C. Beghdadi-Rais, C. Desponds, E. Vargas, S. Herrera, C. D. Reymond, N. Fasel, *Mol. Biochem. Parasitol.* **2000**, *111*, 377.

[23] S.-C. Wu, C. Wang, D. Hansen, S.-L. Wong, *Sci. Rep.* **2017**, *7*, 42849.

[24] a) F. López-Gallego, I. Acebrón, J. M. Mancheño, S. Raja, M. P. Lillo, J. M. Guisán Seijas, *Bioconjugate Chem.* **2012**, *23*, 565; b) I. Acebrón, A. G. Ruiz-Estrada, Y. Luengo, M. D. P. Morales, J. M. Guisán, J. M. Mancheño, *Bioconjugate Chem.* **2016**, *27*, 2734.

[25] I. Angulo, I. Acebrón, B. de Las Rivas, R. Muñoz, I. Rodríguez-Crespo, M. Menéndez, P. García, H. Tateno, I. J. Goldstein, B. Pérez-Agote et al., *Glycobiology* **2011**, *21*, 1349.

[26] M. E. Taylor, K. Drickamer, *Curr. Opin. Struct. Biol.* **2014**, *28*, 14.

[27] J. Henshaw, A. Horne-Bitschy, A. L. van Bueren, V. A. Money, D. N. Bolam, M. Czjzek, N. A. Ekborg, R. M. Weiner, S. W. Hutcheson, G. J. Davies et al., *J. Biol. Chem.* **2006**, *281*, 17099.

[28] F. Cui, S. Dong, X. Shi, X. Zhao, X.-H. Zhang, *Mar. Drugs* **2014**, *12*, 2731.

[29] Z. Fujimoto, *Biosci. Biotechnol. Biochem.* **2013**, *77*, 1363.

[30] Y. Ohta, Y. Nogi, M. Miyazaki, Z. Li, Y. Hatada, S. Ito, K. Horikoshi, *Biosci. Biotechnol. Biochem.* **2004**, *68*, 1073.

[31] Y. Hou, X. Chen, Z. Chan, R. Zeng, *Process Biochem.* **2015**, *50*, 1068.

[32] D. W. Abbott, E. Ficko-Blean, A. L. van Bueren, A. Rogowski, A. Cartmell, P. M. Coutinho, B. Henrissat, H. J. Gilbert, A. B. Boraston, *Biochemistry* **2009**, *48*, 10395.

[33] J. L. Henshaw, D. N. Bolam, V. M. R. Pires, M. Czjzek, B. Henrissat, L. M. A. Ferreira, C. M. G. A. Fontes, H. J. Gilbert, *J. Biol. Chem.* **2004**, *279*, 21552.

[34] V. M. R. Pires, J. L. Henshaw, J. A. M. Prates, D. N. Bolam, L. M. A. Ferreira, C. M. G. A. Fontes, B. Henrissat, A. Planas, H. J. Gilbert, M. Czjzek, *J. Biol. Chem.* **2004**, *279*, 21560.

[35] M. Jam, E. Ficko-Blean, A. Labourel, R. Larocque, M. Czjzek, G. Michel, *FEBS J.* **2016**, *283*, 1863.

[36] B. Pluvinage, J.-H. Hehemann, A. B. Boraston, *J. Biol. Chem.* **2013**, *288*, 28078.

[37] a) H. Hemilä, T. T. Koivula, I. Palva, *Biochim. Biophys. Acta, Lipids Lipid Metab.* **1994**, *1210*, 249; b) G. Manco, E. Adinofi, F. M. Pisani, V. Carratore, M. Rossi, *Protein Pept. Lett.* **1997**, *4*, 375; c) G. Manco, E. Adinolfi, F. M. Pisani, G. Ottolina, G. Carrea, M. Rossi, *Biochem. J.* **1998**, *332*(1), 203; d) G. de Simone, S. Galdiero, G. Manco, D. Lang, M. Rossi, C. Pedone, *J. Mol. Biol.* **2000**, *303*, 761.

[38] a) D. E. Agafonov, K. S. Rabe, M. Grote, Y. Huang, M. Sprinzl, *FEBS Lett.* **2005**, *579*, 2082; b) R. Greifenstein, T. Ballweg, T. Hashem, E. Gottwald, D. Achauer, F. Kirschhöfer, M. Nusser, G. Brenner-Weiß, E. Sedghamiz, W. Wenzel et al., *Angew. Chem. Int. Ed.* **2022**, *61*, e202117144.

[39] B. Zakeri, J. O. Fierer, E. Celik, E. C. Chittock, U. Schwarz-Linek, V. T. Moy, M. Howarth, *Proc. Natl. Acad. Sci. U. S. A.* **2012**, *109*, E690–E697.

[40] T. Peschke, K. S. Rabe, C. M. Niemeyer, *Angew. Chem. Int. Ed.* **2017**, *56*, 2183.

[41] J. Houser, S. Kozmon, D. Mishra, Z. Hammerová, M. Wimmerová, J. Koča, *Chem. - Eur. J.* **2020**, *26*, 10769.

[42] S. Armenta, S. Moreno-Mendieta, Z. Sánchez-Cuapio, S. Sánchez, R. Rodríguez-Sanoja, *Proteins* **2017**, *85*, 1602.

[43] a) M. Mirdita, K. Schütze, Y. Moriwaki, L. Heo, S. Ovchinnikov, M. Steinegger, *Nat. Methods* **2022**, *19*, 679; b) J. Jumper, R. Evans, A. Pritzel,

T. Green, M. Figurnov, O. Ronneberger, K. Tunyasuvunakool, R. Bates, A. Žídek, A. Potapenko et al., *Nature* **2021**, *596*, 583.

[44] C. Taroni, S. Jones, J. M. Thornton, *Protein Eng.* **2000**, *13*, 89.

[45] a) B. Mao, T. Divoux, P. Snabre, *J. Rheol.* **2016**, *60*, 473; b) T. Svedberg, *J. Am. Chem. Soc.* **1924**, *46*, 2673; c) D. Lin, A. L. Kelly, V. Maidannyk, S. Miao, *Food Hydrocolloids* **2020**, *108*, 105998; d) S. B. Shinde, L. Kumar, *Ind. Eng. Chem. Res.* **2021**, *60*, 8565; e) K. Nishinari, Y. Fang, *Food Funct.* **2016**, *7*, 2130.

[46] a) B. Rotman, B. W. Papermaster, *Proc. Natl. Acad. Sci. U. S. A.* **1966**, *55*, 134; b) F.-Y. Ge, L.-G. Chen, X.-L. Zhou, H.-Y. Pan, F.-Y. Yan, G.-Y. Bai, X.-L. Yan, *Dyes Pigm.* **2007**, *72*, 322; c) H. Eshghi, N. Mirzaie, A. Asoodeh, *Dyes Pigm.* **2011**, *89*, 120.

[47] a) X. Li, J. Yang, X. Li, W. Gu, J. Huang, K.-Q. Zhang, *Process Biochem.* **2008**, *43*, 1132; b) W. Gu, X. Li, J. Huang, Y. Duan, Z. Meng, K.-Q. Zhang, J. Yang, *Appl. Microbiol. Biotechnol.* **2011**, *89*, 1797.

[48] W. Gu, J. Yang, Z. Lou, L. Liang, Y. Sun, J. Huang, X. Li, Y. Cao, Z. Meng, K.-Q. Zhang, *PloS One* **2011**, *6*, e16262.

[49] a) C. Wuensch, J. Gross, G. Steinkellner, K. Gruber, S. M. Glueck, K. Faber, *Angew. Chem. Int. Ed.* **2013**, *52*, 2293; b) C. Wuensch, T. Pavkov-Keller, G. Steinkellner, J. Gross, M. Fuchs, A. Hromic, A. Lyskowski, K. Fauland, K. Gruber, S. M. Glueck, K. Faber, *Adv. Synth. Catal.* **2015**, *357*, 1909.

[50] E. Mittmann, S. Gallus, P. Bitterwolf, C. Oelschlaeger, N. Willenbacher, C. M. Niemeyer, K. S. Rabe, *Micromachines* **2019**, *10*, 795.

[51] A. L. van Bueren, C. Morland, H. J. Gilbert, A. B. Boraston, *J. Biol. Chem.* **2005**, *280*, 530.

[52] a) J. Narayanan, J.-Y. Xiong, X.-Y. Liu, *J. Phys. Conf. Ser.* **2006**, *28*, 83; b) N. Pernodet, M. Maaloum, B. Tinland, *Electrophoresis* **1997**, *18*, 55.

[53] M. Maaloum, N. Pernodet, B. Tinland, *Electrophoresis* **1998**, *19*, 1606.

[54] D.-H. Jung, W. Choi, K.-Y. Choi, E. Jung, H. Yun, R. J. Kazlauskas, B.-G. Kim, *Appl. Microbiol. Biotechnol.* **2013**, *97*, 1501.

[55] L. Pesci, M. Baydar, S. Glueck, K. Faber, A. Liese, S. Kara, *Org. Process Res. Dev.* **2017**, *21*, 85.

[56] a) J. M. Salgado, R. Rodríguez-Solana, J. A. Curiel, B. de Las Rivas, R. Muñoz, J. M. Domínguez, *Enzyme Microb. Technol.* **2014**, *22*, 58–59; b) H. Leisch, S. Grosse, K. Morley, K. Abokitse, F. Perrin, J. Denault, P. C. Lau, *Green Process. Synth.* **2013**, *2*, 7; c) I.-Y. Lee, T. G. Volm, J. P. Rosazza, *Enzyme Microb. Technol.* **1998**, *23*, 261.

[57] L. Wenger, J. Hubbuch, *Front. Bioeng. Biotechnol.* **2022**, *10*, 849271.

[58] a) P. Giraudeau, F.-X. Felpin, *React. Chem. Eng.* **2018**, *3*, 399; b) N. Nordin, L. Bordonali, H. Davoodi, N. D. Ratnawati, G. Gygli, J. G. Korvink, V. Badilita, N. MacKinnon, *Angew. Chem. Int. Ed.* **2021**, *60*, 19176.

[59] a) T. Menegatti, I. Plazl, P. Žnidaršič-Plazl, *Chem. Eng. J.* **2024**, *483*, 149317; b) T. Burgahn, P. Pietrek, R. Dittmeyer, K. S. Rabe, C. M. Niemeyer, *ChemCatChem* **2020**, *12*, 2452.

[60] C. Claaßen, K. Mack, D. Rother, *ChemCatChem* **2020**, *12*, 1190.

[61] a) L. Tamborini, P. Fernandes, F. Paradisi, F. Molinari, *Trends Biotechnol.* **2018**, *36*, 73; b) A. I. Benítez-Mateos, M. L. Contente, D. Roura Padrosa, F. Paradisi, *React. Chem. Eng.* **2021**, *6*, 599.

[62] a) Q. Xu, Q. Song, X. Ai, T. J. McDonald, H. Long, S.-Y. Ding, M. E. Himmel, G. Rumbles, *Chem. Commun. (Cambridge, U. K.)* **2009**, 337; b) H. Wernérus, J. Lehtiö, T. Teeri, P.-Å. Nygren, S. Ståhl, *Appl. Environ. Microbiol.* **2001**, *67*, 4678; c) Y. Zhang, L. Wang, J. Chen, J. Wu, *Carbohydr. Polym.* **2013**, *97*, 124.

[63] a) A. Pluen, P. A. Netti, R. K. Jain, D. A. Berk, *Biophys. J.* **1999**, *77*, 542; b) D. G. Gibson, L. Young, R.-Y. Chuang, J. C. Venter, C. A. Hutchison, H. O. Smith, *Nat. Methods* **2009**, *6*, 343; c) S. H. Hansen, T. Kabbeck, C. P. Radtke, S. Krause, E. Krolitzki, T. Peschke, J. Gasmi, K. S. Rabe, M. Wagner, H. Horn et al., *Sci. Rep.* **2019**, *9*, 8933; d) N. Otsu, *IEEE Trans. Syst., Man Cybern.* **1979**, *9*, 62; e) E. Jurrus, D. Engel, K. Star, K. Monson, J. Brandi, L. E. Felberg, D. H. Brookes, L. Wilson, J. Chen, K. Liles et al., *Protein Sci.* **2018**, *27*, 112; f) L. Li, J. O. Fierer, T. A. Rapoport, M. Howarth, *J. Mol. Biol.* **2014**, *426*, 309; g) D. Eisenberg, E. Schwarz, M. Komaromy, R. Wall, *J. Mol. Biol.* **1984**, *179*, 125; h) T. T. Yang, L. Cheng, S. R. Kain, *Nucleic Acids Res.* **1996**, *24*, 4592; i) J. Lasch, *Enzymkinetik. Eine Einführung für Biochemiker, Mediziner, Biologen, Chemiker und Pharmazeuten*, Springer, Berlin, Heidelberg 1987.